# Osmotic swelling behavior of surface-charged ionic microgels

Cite as: J. Chem. Phys. 159, 184901 (2023); doi: 10.1063/5.0161027

Submitted: 7 June 2023 • Accepted: 19 October 2023 •

**Published Online: 9 November 2023** 







Mohammed O. Alziyadi<sup>a)</sup> D and Alan R. Denton<sup>b)</sup>





# **AFFILIATIONS**

Department of Physics, North Dakota State University, Fargo, North Dakota 58108-6050, USA

<sup>a)</sup>Current address: Department of Physics, College of Science and Humanities-Shagra, Shagra University, Riyadh, Saudi Arabia.

b) Author to whom correspondence should be addressed: alan.denton@ndsu.edu

#### **ABSTRACT**

In recent years, ionic microgels have garnered much attention due to their unique properties, especially their stimulus-sensitive swelling behavior. The tunable response of these soft, permeable, compressible, charged colloidal particles is increasingly attractive for applications in medicine and biotechnologies, such as controlled drug delivery, tissue engineering, and biosensing. The ability to model and predict variation of the osmotic pressure of a single microgel with respect to changes in particle properties and environmental conditions proves vital to such applications. In this work, we apply both nonlinear Poisson-Boltzmann theory and molecular dynamics simulation to ionic microgels (macroions) in the cell model to compute density profiles of microions (counterions, coions), single-microgel osmotic pressure, and equilibrium swelling ratios of spherical microgels whose fixed charge is confined to the macroion surface. The basis of our approach is an exact theorem that relates the electrostatic component of the osmotic pressure to the microion density profiles. Close agreement between theory and simulation serves as a consistency check to validate our approach. We predict that surface-charged microgels progressively deswell with increasing microgel concentration, starting well below close packing, and with increasing salt concentration, in qualitative agreement with experiments. Comparison with previous results for microgels with fixed charge uniformly distributed over their volume demonstrates that surface-charged microgels deswell more rapidly than volume-charged microgels. We conclude that swelling behavior of ionic microgels in solution is sensitive to the distribution of fixed charge within the polymer-network gel and strongly depends on bulk concentrations of both microgels and salt ions.

Published under an exclusive license by AIP Publishing. https://doi.org/10.1063/5.0161027

# I. INTRODUCTION

Microgels are soft colloidal particles, made of a cross-linked polymer network gel, that become swollen in a good solvent.1 Depending on the procedure for their chemical synthesis,<sup>5</sup> microgels can be designed to swell/deswell in response to external parameters, such as temperature, pH, and ionic strength.<sup>6</sup> Swelling behavior depends on mechanical (elastic) properties of the gel and polymersolvent interactions.<sup>7,8</sup> When microgels are dispersed in a polar solvent (e.g., water), dissociation of counterions from the polymer chains can turn the particles into colloidal macroions with a fixed (immobile) charge. 9,10 Swelling behavior of ionic microgels is influenced by electrostatic interactions between fixed charge, counterions, and coions (from added salt).<sup>11</sup> Microgels and, in particular, ionic microgels have been extensively investigated due to their applications in biomedical, food, pharmaceutical, and petroleum industries.1

The swelling behavior of microgels, in contrast to that of bulk gels, 17-20 is fundamentally determined by the single-particle osmotic pressure, defined as the difference in pressure between the interior and exterior regions.<sup>21,22</sup> In thermodynamic equilibrium, this single-particle osmotic pressure must vanish, achieved only through a delicate balance between electrostatic, elastic, and mixing entropic contributions. In concentrated suspensions of microgels, equilibrium particle sizes respond also to self-crowding, as each particle adjusts its internal degrees of freedom to the local environment, with relevance for macroscopic phase behavior.

Swelling properties of microgels (ionic and nonionic) have been investigated by several complementary experimental methods, including light scattering,<sup>23</sup> neutron scattering,<sup>2</sup> osmometry, 31,32 and dielectric spectroscopy. 33 Compressible microgels and suspensions thereof have been modeled by a variety of theoretical methods, including mean-field theories, <sup>34–38</sup> equation theories, <sup>39</sup> effective interaction theories, <sup>40–43</sup>

model-based theories.<sup>21,22,44</sup> Simulation studies have applied various molecular dynamics<sup>45–49</sup> and Monte Carlo<sup>42,50–53</sup> methods. From past work, swelling behavior is known to depend sensitively on single-particle properties, including the distribution of cross-links in the polymer network comprising the gel.<sup>54,55</sup> In general, the lower the cross-link concentration, the softer and more compressible the particles, although the spatial distribution of cross-links is also relevant.

Less well understood is the connection between swelling and the distribution of fixed charge on the polymer network. In chemical synthesis protocols developed to produce ionic microgels, the fixed charge distribution can be controlled, to some extent, by adjusting the concentration and chemical species of the initiator for the polymerization reaction in the synthesis. In some microgel systems, initiator molecules themselves are charged and tend to deposit near the particle's periphery, yielding a surface-localized fixed charge. <sup>32,56-59</sup> How in detail the fixed charge distribution affects osmotic pressure and equilibrium swelling of ionic microgels is a largely unresolved question.

To address the question of how fixed charge distribution influences swelling of microgels, we have developed theoretical and computational modeling methods for ionic microgels and applied them to macroions with fixed charge confined to their surface. Comparison of predictions for this idealized model with corresponding results from our earlier studies of microgels with fixed charged uniformly distributed throughout their volume<sup>21,22</sup> contrasts the sensitivity of swelling to fixed charge distribution between two extreme distributions. Our approach is based on fundamental statistical mechanical relations for the electrostatic component of the single-microgel osmotic pressure that accurately account for counterion and coion correlations. Building on our previous work, this paper describes the swelling of ionic microgels as a competition between electrostatic and gel contributions to the osmotic pressure and demonstrates the sensitivity of swelling to the fixed charge distribution.

In Sec. II, we define the primitive and cell models of ionic microgels, which are the foundation for our study. In Sec. III, we review our theory of microgel swelling, deriving the electrostatic component of the single-microgel osmotic pressure from a partition function and approximating the gel contribution using the Flory–Rehner theory of polymer networks. Section IV outlines our computational implementation of the swelling theory via Poisson–Boltzmann theory and molecular dynamics simulation. Section V presents numerical results for counterion density profiles, single-microgel osmotic pressure, and equilibrium swelling ratios of surface-charged microgels. We compare and contrast the swelling behavior with that of volume-charged microgels and discuss the influence of added salt. Finally, Sec. VI summarizes our results and concludes with suggestions for future work.

## II. MODELS

# A. Primitive model

Theoretical descriptions of polyelectrolyte solutions and charge-stabilized colloidal suspensions are often based on the primitive model, which approximates the solvent as an implicit medium – a dielectric continuum characterized entirely by a dielectric constant  $\epsilon$  – and considers explicitly only the charged

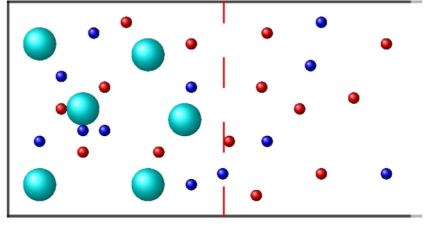
species.  $^{60,61}$  Within this coarse-grained model, we consider an aqueous suspension of  $N_m$  ionic microgels, each composed of a microscopic cross-linked network of polymer chains, dispersed in a solvent (water) of volume V at temperature T, as depicted in Fig. 1.

We model ionic microgels as spherical macroions of dry radius  $a_0$ , swollen radius a, and fixed charge -Ze, resulting from dissociation of Z monovalent counterions (of charge e) from the polymer chains. The swollen microgels are assumed to be permeable to solvent, counterions, and coions (see Fig. 1). Assuming that a microgel in its dry (unswollen) state comprises randomly close-packed spherical monomers, the number of monomers per microgel is related to the monomer radius  $r_{\rm mon}$  by  $N_{\rm mon} = 0.63 (a_0/r_{\rm mon})^3$ .

In experiments, the distribution of fixed charge can be controlled, to some extent, via the chemical synthesis protocol. In some systems, e.g., poly-N-isopropilacrylamide (pNIPAM) microgels, the fixed charges originate from the initiator species for the polymerization reaction in the synthesis, which are believed to end up localized near the particle surface. <sup>56–59</sup> We consider here the ideal case that the fixed charge is strictly confined to and uniformly distributed over the particle surface, with number density described by a Dirac delta-function,

$$n_f(r) = \frac{Z}{4\pi a^2} \delta(r - a),\tag{1}$$

where Z is the microgel valence and r is the radial distance from the microgel center. Elsewhere,  $^{62,63}$  we investigated swelling of ionic



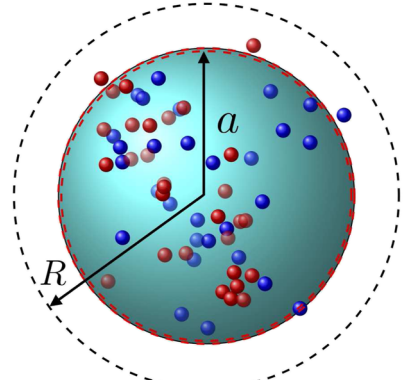


**FIG. 1.** Schematic drawings of (top) primitive model of a suspension of spherical ionic microgels (large cyan spheres) and microions (small red and blue spheres) dispersed in a dielectric continuum solvent and (bottom) cell model of a surface-charged microgel of swollen radius *a* confined to a spherical cell of radius *R* with counterions (red) and coions (blue).

microcapsules, whose fixed charge is spread throughout a spherical shell of a hollow microgel. In contrast, the microgels studied here are not hollow, but are completely filled with hydrogel. The microions are modeled as monovalent point charges of valence  $z_{\pm}=\pm 1$ . In Donnan equilibrium with a 1:1 electrolyte (salt) reservoir, the suspension contains  $N_s$  dissociated salt ion pairs, which contribute equal numbers of coions and additional counterions to the solution. Electroneutrality of the suspension dictates the total numbers of counterions and coions as  $N_+=Z+N_s$  and  $N_-=N_s$ , respectively, for a total of  $N_\mu=Z+2N_s$  microions.

#### B. Cell model

The cell model, originally proposed by Wigner and Seitz to calculate electronic properties of solids, <sup>64,65</sup> can also be applied to polyelectrolyte solutions, as first recognized by Marcus, <sup>66</sup> charge-stabilized colloidal suspensions, <sup>60</sup> and hydrogels. <sup>67</sup> In this context, the cell model reduces a system of many macroions dispersed in an electrolyte solution to a single macroion confined to a cell of like shape, along with stoichiometric numbers of counterions and coions (Fig. 1). This relatively simple model, by explicitly including microions, retains microion-microion and microion-macroion interactions, but sacrifices macroion-macroion interactions and correlations, aside from a mean-field contribution to the total electrostatic energy.

In the cell model of an ionic microgel suspension, a swollen, spherical microgel (macroion) of radius a, with radially symmetric fixed charge density  $n_f(r)$ , is centered in a spherical cell of radius R, which determines the suspension volume fraction  $\phi = (a/R)^3$ . From spherical symmetry, the electrostatic potential and microion densities  $n_\pm(r)$  depend on only the radial distance r from the center of the cell. Further, electroneutrality requires that the electric field vanishes at the cell boundary (r = R).

The model system is governed by a Hamiltonian H, which we assume can be separated, <sup>42</sup> according to

$$H = H_g + H_e, (2)$$

into a "gel" Hamiltonian  $H_g$ , associated with mutual interactions among monomers of the cross-linked polymer chains and the solvent molecules, and an "electrostatic" Hamiltonian  $H_e$ , which includes the Coulomb energies of interaction between ions (fixed and mobile). The gel Hamiltonian incorporates elastic and mixing degrees of freedom of a polymer network in solution. The electrostatic Hamiltonian further decomposes, according to

$$H_e = U_m(a) + U_{m\mu}(\{\mathbf{r}\}; a) + U_{\mu\mu}(\{\mathbf{r}\}),$$
 (3)

whose three terms account, respectively, for the electrostatic self-energy of a microgel and macroion-microion and microion-microion pair interaction energies, which depend on the microion coordinates,  $\{\mathbf{r}\} = \{\mathbf{r}_1, \dots, \mathbf{r}_{N_\mu}\}$ . Note that the first two terms on the right side of Eq. (3) are functions of the microgel radius, and thus vary with swelling of the polymer network.

A surface-charged spherical macroion has electrostatic selfenergy, in thermal  $(k_BT)$  units,

$$\beta U_m(a) = Z^2 \frac{\lambda_B}{2a},\tag{4}$$

where the Bjerrum length,  $\lambda_B \equiv \beta e^2/\epsilon$ , is the distance at which two elementary charges e have a Coulomb energy equal to the thermal energy  $k_BT \equiv 1/\beta$ . The microgel-microion interaction energy can be expressed as

$$U_{m\mu}(\{\mathbf{r}\};a) = \sum_{i=1}^{N_{+}} v_{m+}(\mathbf{r}_{i};a) + \sum_{i=1}^{N_{-}} v_{m-}(\mathbf{r}_{i};a),$$
 (5)

where  $v_{m\pm}$  are the macroion-counterion and macroion-coion electrostatic pair potentials:

$$\beta v_{m\pm}(r;a) = \begin{cases} \mp Zz\lambda_B/r, & r > a \\ \mp Zz\lambda_B/a, & r \le a. \end{cases}$$
 (6)

The fact that the macroion-microion pair potentials depend on the microgel radius a has direct implications for swelling of ionic microgels, as discussed below in Sec. III. In passing, we note that, in the full primitive model of a suspension of many microgels, the electrostatic Hamiltonian would include, in addition to the three terms in Eq. (3), a fourth term accounting for microgel-microgel electrostatic interactions,

$$U_{mm}(a) = \sum_{i < j=1}^{N_m} v_{mm}(r_{ij}; a).$$
 (7)

For spherical microgels, however, the dependence of the bare Coulomb microgel-microgel pair potential  $v_{mm}(r; a)$  on microgel radius arises only when the microgels overlap. For other shapes of microgels, pair interactions do not have this symmetry property, and would depend on the orientations of the particles at all separations.

In the cell model, microgel-microgel electrostatic interactions are implicitly accounted for through the boundary condition that the electric field vanishes at the cell edge. The focus on a single microgel of course necessitates neglect of microgel-microgel correlations. In an alternative approach, microion degrees of freedom are averaged over (traced out of the partition function), reducing the multi-component mixture to an effective one-component model of pseudo-macroions that interact via an *effective* screened-Coulomb (Yukawa) pair potential. <sup>40–42</sup> In this multi-centered model, effective pair interactions influence swelling at densities well below close packing, corresponding to nearest-neighbor separations comparable to the Debye screening length. Remarkably, as shown in Ref. 42 for volume-charged microgels, the cell and one-component models predict very similar swelling behavior up to close-packing densities.

#### III. THEORY OF MICROGEL SWELLING

Swelling of microgels is governed by the single-microgel osmotic pressure  $\pi_m$ , defined as the difference in pressure between the interior and exterior of the microgel. This single-microgel property is to be distinguished from the osmotic pressure of a microgel suspension  $\pi_s$ , which is a bulk (macroscopic) property. In a canonical ensemble description, in which the suspension is assumed to be closed (i.e., has a fixed number of particles), the single-microgel osmotic pressure is thermodynamically defined as a derivative of the

Helmholtz free energy per microgel F with respect to the microgel volume  $v_m = 4\pi a^3/3$ . Within the spherical cell model,

$$\pi_m = -\left(\frac{\partial F}{\partial v_m}\right)_{N_w,R,T} = -\frac{1}{4\pi a^2} \left(\frac{\partial F}{\partial a}\right)_{N_w,R,T},\tag{8}$$

revealing the connection between  $\pi_m$  and the variation of the free energy with swollen radius. In contrast, the suspension osmotic pressure depends on the variation of the free energy with cell volume or radius,

$$\pi_s = -\left(\frac{\partial F}{\partial V}\right)_{N-T} = -\frac{1}{4\pi R^2} \left(\frac{\partial F}{\partial R}\right)_{N-T}.$$
 (9)

The cell theorem<sup>66,68</sup> further relates  $\pi_s$  to the total microion density at the cell boundary:

$$\beta \pi_s = n_+(R) + n_-(R).$$
 (10)

In passing, we note that the results derived below can be equally well obtained within the semi-grand canonical ensemble, in which the suspension is free to exchange microions with a salt reservoir, which describes the condition of Donnan equilibrium. <sup>21,22</sup>

Separation of the Hamiltonian into electrostatic and gel terms [Eq. (2)] implies that the canonical partition function  $\mathcal{Z}$  factorizes, according to  $\mathcal{Z} = \mathcal{Z}_e \mathcal{Z}_g$ , into electrostatic and gel factors. Within the spherical cell model, the electrostatic partition function takes the form

$$\mathcal{Z}_{e}(N_{\mu}, a, R, T) \propto \prod_{i=1}^{N_{\mu}} \int_{0}^{R} dr_{i} r_{i}^{2} e^{-\beta H_{e}},$$
 (11)

where the position integrals cover possible configurations of all microions within the cell. Factorization of the partition function implies decomposition of the free energy,

$$F = -k_B T \ln \mathcal{Z} = F_g + F_e, \tag{12}$$

into (1) a gel contribution,  $F_g = -k_B T \ln Z_g$ , associated with short-range monomer-monomer interactions, mixing entropy of the polymer-solvent mixture, and conformational entropy of the polymer chains, and (2) an electrostatic contribution,  $F_e = -k_B T \ln Z_e$ , due to long-range (Coulomb) ion-ion interactions. Correspondingly, the single-microgel osmotic pressure separates, via

$$\pi_m(\alpha) = \pi_g(\alpha) + \pi_e(\alpha), \tag{13}$$

into gel and electrostatic contributions,  $\pi_g(\alpha)$  and  $\pi_e(\alpha)$ , both being functions of the microgel linear swelling ratio  $\alpha \equiv a/a_0$ .

In thermodynamic equilibrium, a microgel swells until its osmotic pressure vanishes, i.e.,  $\pi_m(\alpha) = 0$ . As we showed in previous work, <sup>22</sup> this condition ensures continuity of the radial component of the total pressure tensor across the microgel surface in equilibrium. Note that the individual contributions to  $\pi_m$  may be nonzero, as long as their sum vanishes in equilibrium.

As an approximation for the gel contribution to the free energy, we adopt the mean-field Flory–Rehner theory of polymer networks,  $^{7,69,70}$  which combines polymer-solvent interactions and mixing entropy with elastic free energy of the network. For a microgel of swollen radius a and dry radius  $a_0$ , composed of

 $N_{\text{mon}}$  monomers and  $N_{\text{ch}}$  distinct chains (cross-linked into a network) in a solvent, the gel free energy takes the form

$$\beta F_g(\alpha) = N_{\text{mon}} [(\alpha^3 - 1) \ln (1 - \alpha^{-3}) + \chi (1 - \alpha^{-3})]$$

$$+ \frac{3}{2} N_{\text{ch}} (\alpha^2 - \ln \alpha - 1),$$
(14)

where  $\chi$  is the Flory solvency parameter, associated with polymer-polymer, polymer-solvent, and solvent-solvent interactions. The corresponding gel contribution to the single-microgel osmotic pressure can be written as

$$\beta \pi_g(\alpha) v_m = -N_{\text{mon}} \left[ \alpha^3 \ln (1 - \alpha^{-3}) + \chi \alpha^{-3} + 1 \right] - N_{\text{ch}}(\alpha^2 - 1/2).$$
 (15)

The electrostatic contribution to the single-microgel osmotic pressure can be derived in principle from the electrostatic contribution to the free energy via<sup>38</sup>

$$\pi_e = -\frac{1}{4\pi a^2} \left(\frac{\partial F_e}{\partial a}\right)_{N_u, R, T}.$$
 (16)

However, this expression is only as accurate as the approximation for the free energy. Alternatively, from Eqs. (4) and (5),  $\pi_e$  can be expressed as

$$\pi_e = -\frac{1}{4\pi a^2} \left( \frac{\partial U_m(a)}{\partial a} + \left( \frac{\partial U_{m\mu}(a)}{\partial a} \right) \right)_{N_n R T}, \tag{17}$$

where angular brackets denote an ensemble average over configurations of the microions. Applying the latter approach to ionic microgels requires specifying a model for the fixed charge distribution. Assuming a surface-charged microgel and using the appropriate macroion-microion interaction potentials [Eq. (7)], the second term on the right side of Eq. (17) takes the explicit form

$$\beta \left( \frac{\partial U_{m\mu}(a)}{\partial a} \right) = \frac{Z\lambda_B}{a^2} \left( \sum_{i(r_i \le a)} z_i \right), \tag{18}$$

where the sum over i ( $i = \pm$  for counterions or coions) includes only microions inside the microgel. Finally, substituting the self energy [Eq. (4)] and the expression from Eq. (18) into Eq. (17), we obtain the electrostatic component of the single-microgel osmotic pressure:

$$\beta \pi_e v_m = \frac{Z \lambda_B}{3a} \left( \frac{Z}{2} - \langle N_+ \rangle + \langle N_- \rangle \right), \tag{19}$$

where

$$\langle N_{\pm} \rangle = 4\pi \int_0^a dr r^2 n_{\pm}(r) \tag{20}$$

represent mean numbers of counterions and coions *inside* the microgel, ensemble averaged over microion configurations.<sup>22</sup> The first term on the right side of Eq. (19) derives from the microgel self-energy, while the remaining terms are associated with the microion distribution. Equations (13), (15), and (19), combined with the condition  $\pi_m(\alpha) = 0$ , determine a microgel's equilibrium swollen size. In previous work,<sup>22</sup> we showed that our expression for the electrostatic component of the single-microgel osmotic pressure in the cell

model is equivalent to the jump at the microgel surface in the radial component of the electrostatic pressure tensor. 71,72

Note that Eq. (19), akin to the cell theorem for the suspension osmotic pressure [Eq. (10)], is an *exact* theorem within the cell model, fully accounting for microion correlations. In multi-center models of microgel suspensions, these theorems cease to be exact, as they neglect osmotic pressure contributions from microgel-microgel pair interactions and correlations. Nevertheless, since these pair interactions depend on microgel size only for overlapping microgels, Eq. (19) gives a reasonable approximation for dilute suspensions, and should be accurate even for concentrations approaching close-packing. <sup>42</sup>

## IV. COMPUTATIONAL METHODS

# A. Poisson-Boltzmann theory in the cell model

Practical implementation of the theory described in Sec. III to model equilibrium swelling of ionic microgels requires estimates for the mean numbers of counterions and coions inside a microgel. Within the cell model, a convenient method for computing  $\langle N_{\pm} \rangle$  is Poisson–Boltzmann (PB) theory. Based on a mean-field approximation that neglects microion-microion correlations, this theory can be rigorously derived, e.g., via calculus of variations<sup>22</sup> and classical density-functional theory.<sup>73</sup>

Defining  $\psi(r) \equiv \beta e \phi(r)$  as the reduced (dimensionless) form of the electrostatic potential  $\phi(r)$ , where r is the radial distance from the center of the cell, the Poisson equation can be expressed as

$$\nabla^2 \psi(r) = -4\pi \lambda_B [n_+(r) - n_-(r) - n_f(r)], \tag{21}$$

where the right-hand side includes the total charge density, including the mobile microions and the fixed charge on the microgel. For a suspension in Donnan equilibrium with a salt reservoir of average salt density  $n_0$ , the mean-field Boltzmann approximation for the microion equilibrium densities takes the form

$$n_{\pm}(r) = n_0 \exp\left[\mp \psi(r)\right]. \tag{22}$$

Combining Eqs. (21) and (22) yields the (nonlinear) Poisson–Boltzmann equation:

$$\psi''(r) + \frac{2}{r}\psi'(r) = \kappa^2 \sinh \psi(r) + 4\pi\lambda_B n_f(r),$$
 (23)

where  $\kappa \equiv \sqrt{8\pi\lambda_B n_0}$  is the Debye screening constant. For a closed, salt-free suspension, with fixed counterion density, the PB equation takes the alternate form

$$\psi''(r) + \frac{2}{\pi}\psi'(r) = -\tilde{\kappa}^2 \exp\left[-\psi(r)\right] + 4\pi\lambda_B n_f(r),$$
 (24)

where  $\tilde{\kappa} \equiv \sqrt{4\pi\lambda_B\tilde{n}_+}$  is the effective screening constant within the suspension and  $\tilde{n}_+$  is the counterion number density at  $\psi = 0$ .

In the case of a microgel with fixed charge confined to its surface, we substitute Eq. (1) into Eq. (23) to obtain

$$\psi''(r) + \frac{2}{r}\psi'(r) = \kappa^2 \sinh \psi(r) + \frac{Z\lambda_B}{a^2}\delta(r-a), \qquad (25)$$

which is the PB equation in the spherical cell model for a suspension of surface-charged microgels in Donnan equilibrium. This equation is subject to the boundary conditions that the electric field must vanish at the center of the cell,  $\psi'(0) = 0$  (by symmetry), and on the cell boundary,  $\psi'(R) = 0$  (by electroneutrality). Applying these boundary conditions, we numerically solved Eq. (25) for  $\psi(r)$  inside and outside the microgel and matched the solutions in the two regions at the microgel surface to ensure continuity of the potential and the correct discontinuity of the electric field at r = a:

$$\lim_{\delta \to 0} \left[ \psi'(a+\delta) - \psi'(a-\delta) \right] = \frac{Z\lambda_B}{a^2}.$$
 (26)

From our solution for  $\psi(r)$ , we computed the microion density profiles from Eq. (22) and the electrostatic component of the single-microgel osmotic pressure from Eqs. (19) and (20).

Previously, we showed<sup>22</sup> that a careful analysis of the pressure tensor within the cell model implementation of PB theory relates the electrostatic component of the single-microgel osmotic pressure to the discontinuity in the radial component of the electrostatic pressure tensor at the microgel surface:

$$\beta \pi_e = \frac{Z}{8\pi a^2} \lim_{\delta \to 0} \left| \psi'(a+\delta) + \psi'(a-\delta) \right|. \tag{27}$$

We further showed that this expression is equivalent to our exact statistical mechanical relation [Eq. (19)].

# B. Molecular dynamics simulations

An independent means of computing the microion density distributions is molecular simulation. To validate our PB theory predictions, we implemented and performed canonical ensemble molecular dynamics (MD) simulations to compute  $\langle N_{\pm} \rangle$  within the cell model. Using the large-scale atomic/molecular massively parallel simulator (LAMMPS) package,  $^{74,75}$  we simulated a collection of counterions (and coions), interacting via a hybrid pair potential, combining a long-range Coulomb pair potential with a short-range, repulsive, cut-off Lennard-Jones pair potential. To mimic the influence of a central, spherical ionic microgel, we applied a radial "external" force,  $^{21}$ 

$$F_{\text{ext}}(r) = \mp \frac{Ze^2}{4\pi\epsilon} \begin{cases} r/a^3, & r \le a, \\ 1/r^2, & r > a, \end{cases}$$
 (28)

which is attractive/repulsive  $(\mp)$  for counterions/coions.

The microions were initialized on the sites of an FCC lattice with random velocities consistent with a constant temperature, and confined to a spherical region by a repulsive Lennard-Jones wall force. During the simulations, trajectories of the mobile microions were computed by numerically integrating Newton's equations of motion using the velocity-Verlet algorithm. The average temperature was held constant via a Nosé–Hoover thermostat. After equilibrating the system for  $10^6$  time steps (fs), we continued each run for another  $10^8$  steps, during which time we collected statistics.

In all MD simulations and PB calculations, the following system parameters were kept fixed: Bjerrum length  $\lambda_B$ , cell radius R, microgel dry radius  $a_0$ , cross-link fraction, dry volume fraction  $\phi_0$ , valence Z, and Flory solvency parameter  $\chi$ . For a given value of Z, the total number of dissociated monovalent counterions was  $N_+ = Z$  to maintain electroneutrality. Figure 2 shows a typical snapshot from one of our simulations of an ionic microgel and counterions.

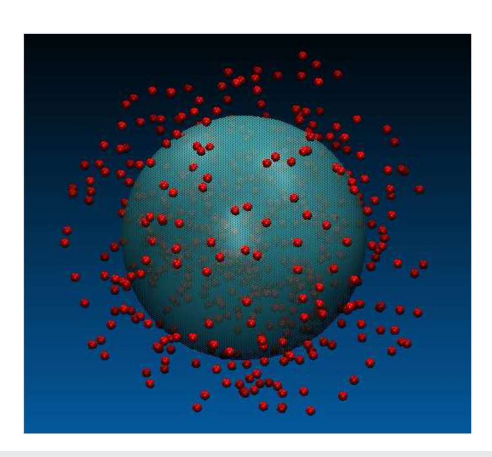


**FIG. 2.** Snapshot from MD simulation of an ionic microgel (cyan sphere) and mobile counterions (red spheres).

#### V. RESULTS AND DISCUSSION

To explore the dependence of equilibrium swelling behavior of ionic microgels on fixed charge distribution, we implemented the models, theory, and computational methods described in Secs. II–IV. We consider here aqueous suspensions at temperature T=293 K, with a uniform Bjerrum length,  $\lambda_B=0.714$  nm, assuming equal dielectric constants inside and outside of the microgels. As representative system parameters, we chose a dry microgel radius of  $a_0=10$  nm, corresponding to  $N_{\rm mon}=2\times10^5$  monomers of radius  $r_{\rm mon}\simeq 0.15$  nm; number of chains  $N_{\rm ch}=100$ , corresponding to average cross-link fraction  $x=0.5N_{\rm ch}/N_{\rm mon}=2.5\times10^{-4}$ ; valence Z=1000; and Flory solvency parameter  $\chi=0.5$ .

In previous work,  $^{21}$  we developed a similar modeling approach and applied it to spherical ionic microgels carrying fixed charge uniformly distributed over their volume. We numerically solved the PB equation and performed MD simulations to compute average microion number density profiles, and thus average numbers of interior microions  $\langle N_{\pm} \rangle$ . From the resulting electrostatic component of the single-microgel osmotic pressure  $\pi_e$ , we determined equilibrium swelling ratios. Here, we apply a comparable approach to microgels with fixed charge uniformly distributed over their surfaces.

Figure 3 shows our results for average counterion number density profiles inside and outside of a surface-charged microgel of swollen radius a = 25 nm (swelling ratio  $\alpha = 2.5$ ) in the spherical cell model with no salt. Excellent agreement between predictions of PB theory and data from our MD simulations over a range of dry volume fractions serves to validate our implementations of both methods. Consistent with the boundary conditions on the PB equation for the electrostatic potential, the counterion density profiles are relatively flat near the microgel center (r = 0) and the cell edge (r = R), where the electric field vanishes. Furthermore, the counterion density peaks at the surface of the microgel, where the electric field is highest. The cusp in the  $n_+(r)$  curve at r = a is a consequence of the strict confinement of the fixed charge to the particle surface.

With increasing dry volume fraction, the maxima of the  $n_+(r)$  curves (at r=a) increase. This trend is to be expected, since the counterion density closely tracks the electrostatic potential

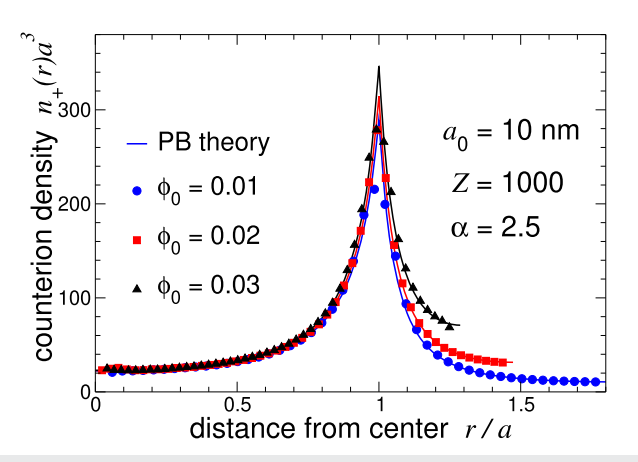


**FIG. 3.** Counterion number density profiles around a surface-charged ionic microgel of dry radius  $a_0=10$  nm, swollen radius a=25 nm, and valence Z=1000 in a salt-free aqueous solvent at room temperature ( $\lambda_B=0.714$ ) in the spherical cell model. For dry volume fractions  $\phi_0=0.01$ , 0.02, and 0.03, predictions of PB theory (solid curves) agree closely with MD simulation data (symbols). The corresponding swollen volume fractions are  $\phi=0.15625$ , 0.3125, and 0.46875.

[Eq. (22)], whose magnitude  $|\psi(r)|$  attains a maximum at the surface and whose surface value  $|\psi(a)|$  increases with increasing  $\phi_0$ . This increase in peak height reflects a stronger attraction of counterions to the surface at higher microgel volume fractions. Furthermore, the average number of interior counterions  $\langle N_+ \rangle$  [Eq. (20)] also increases with increasing  $\phi_0$ , a trend that results largely from the corresponding decrease in exterior volume. Interestingly, inside and away from the microgel surface, the counterion density profile changes relatively little. This behavior is expected, as the environment of the interior counterions is weakly affected by a change in volume outside of the microgel as  $\phi_0$  changes. Note that at low volume fractions (dilute conditions) the counterion density near the microgel center is higher than at the cell edge, while at higher volume fractions this relation is reversed. In previous work, 62,63 found that distributing the fixed charge over the shell thickness of a spherical microcapsule smooths and broadens the counterion density profile.

As discussed in Sec. IV, the electrostatic component of the single-microgel osmotic pressure  $\pi_e$  involves contributions both from the self-energy of the microgel fixed charge and from the density distributions of the mobile microions. Numerically integrating the microion density profiles over the volume of the swollen microgel yields the average numbers of interior microions  $\langle N_{\pm} \rangle$  [Eq. (20)]. In the salt-free case, substituting the average number of interior counterions  $\langle N_+ \rangle$  into Eq. (19) gives  $\pi_e$  for a microgel of a given swollen radius. Repeating these calculations for different swollen radii, we computed  $\pi_e$  over a range of microgel swelling ratios and dry volume fractions. Figure 4 shows our results for  $\pi_e$  vs  $\alpha$  for several values of  $\phi_0$ , together with the gel component of the singlemicrogel osmotic pressure [Eq. (15)], which is independent of  $\phi_0$ . Again, our predictions from PB theory are in very close agreement with our simulation data, as is to be expected, since  $\pi_e$  is directly determined by the value of  $\langle N_+ \rangle$ .

For a given microgel swollen radius, as the dry volume fraction increases (from  $\phi_0$  = 0.01 to 0.05), the electrostatic component of

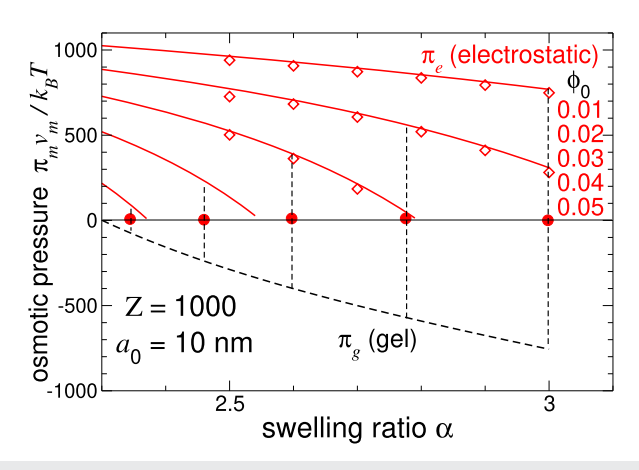


**FIG. 4.** Electrostatic and gel components of single-microgel osmotic pressure vs swelling ratio  $\alpha$  for surface-charged microgels in salt-free aqueous suspensions of dry volume fraction  $\phi_0=0.01-0.05$  in the spherical cell model for same system parameters as in Fig. 3. The electrostatic component  $\pi_e$  from PB theory (solid red curves) agrees closely with MD simulation data (open red symbols). The gel component  $\pi_g$  (dashed black curve) is computed from Flory–Rehner theory [Eq. (15)]. At equilibrium swelling, the total microgel osmotic pressure vanishes:  $\pi_m=\pi_e+\pi_g=0$  (filled symbols).

the single-microgel osmotic pressure steadily decreases (red curves and symbols in Fig. 4). This trend can be attributed to the progressive neutralization of ionic microgels with increasing concentration of the suspension, as counterions become increasingly confined within the microgel, i.e., as  $\langle N_+ \rangle$  increases. (Note that in the cell model, increasing  $\phi_0$  implies decreasing cell radius R.) Furthermore, for these system parameters, at a given concentration,  $\pi_e$  also monotonically decreases with increasing swelling ratio (i.e., with increasing swollen radius for a fixed cell radius). At sufficiently large  $\alpha$ , the self-energy and counterion contributions to the electrostatic osmotic pressure balance and  $\pi_e = 0$ . Thus, concentrating the suspension (increasing  $\phi_0$ ) or enlarging the microgels (increasing  $\alpha$ ) weakens electrostatic effects (lowering  $\pi_e$ ), which tends to promote deswelling and expulsion of solvent. Conversely, decreasing  $\phi_0$  or α enhances electrostatic effects, which favors swelling and absorption of solvent.

The gel component of the single-microgel osmotic pressure  $\pi_g$  [Eq. (15)], associated with mixing entropy and elasticity, counters the electrostatic component. Recall that the total single-microgel osmotic pressure  $\pi_m$  – the sum of the electrostatic and gel components [Eq. (13)] – vanishes when a microgel attains its equilibrium swollen size. An uncharged (nonionic) microgel is in equilibrium when  $\pi_g$  (dashed black curve in Fig. 4) itself vanishes (at  $\alpha \simeq 2.3$  in this case). With increasing swelling ratio,  $\pi_g$  monotonically decreases, becoming negative when  $\alpha > 2.3$ , but with a qualitatively different  $\alpha$  dependence. While a nonionic microgel would be out of equilibrium beyond this swelling ratio, an ionic microgel can be stabilized by the electrostatic component of the osmotic pressure, here arising from the fixed surface charge. The red dots in Fig. 4 mark the equilibrium size of the microgel, at which  $\pi_g(\alpha) + \pi_e(\alpha) = 0$ , for different dry radii.

The resulting equilibrium swelling behavior is summarized in Fig. 5, which shows progressive deswelling with increasing  $\phi_0$ . Over

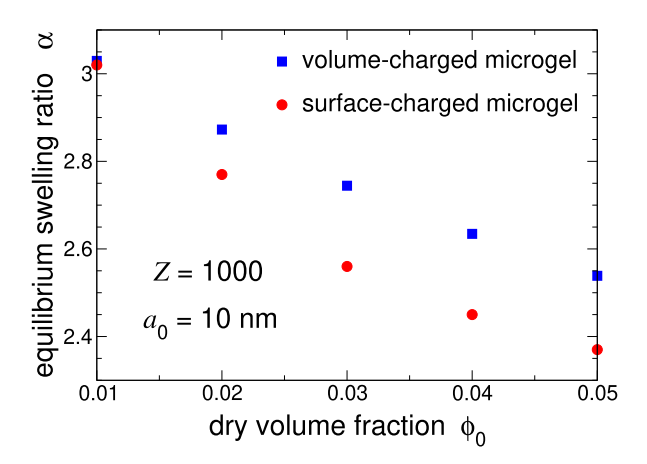


**FIG. 5.** Equilibrium swelling ratio  $\alpha$  vs dry volume fraction  $\phi_0$  for salt-free aqueous suspensions of surface-charged (red circles) and volume-charged (blue squares) microgels in the spherical cell model for same system parameters as in Fig. 3, illustrating stronger deswelling of surface-charged microgels. Over this range of  $\phi_0$ , the swollen volume fraction,  $\phi=\alpha^3\phi_0$ , varies (nonlinearly) from about 0.28–0.67 for surface-charged microgels.

this range of dry volume fraction, the swollen volume fraction,  $\phi = \alpha^3 \phi_0$ , varies (nonlinearly) from about 0.28–0.67 for surface-charged microgels, remaining below close-packing of spheres. Thus, the deswelling of these ionic microgels is driven mainly by electrostatic effects, rather than by steric interparticle interactions. With increasing  $\phi_0$ , increasingly more counterions reside, on average, inside the microgel, lowering the contribution of microgel-counterion electrostatic interactions to the osmotic pressure [Eq. (18)], and thus inducing deswelling.

Our predictions of progressive deswelling of ionic microgels with increasing concentration are qualitatively consistent with experimental observations of deswelling, e.g., of pNIPAM and poly(vinylpyridine) microgels. 31,32,56-59 In particular, pNIPAM microgels, whose fixed charge is localized near the particle periphery, similar to our surface-charged model, exhibit such a deswelling response. 56-59 A direct quantitative comparison between theory and experiment may be possible, but is complicated by the challenge of precisely measuring the fixed charge and by the neglect in our model of any variation of fixed charge with microgel concentration.

Scotti *et al.*<sup>56-58</sup> have suggested a model of ionic microgels in which counterions that are closely associated with fixed charge, i.e., quasi-bound to the surface with an electrostatic potential energy  $\gtrsim k_BT$ , may, at sufficiently high microgel concentration, be released (i.e., become free) and thereby contribute to the osmotic pressure of the suspension. Such a release of counterions would alter the effective fixed charge of the microgels. Since our coarse-grained, cell-model-based approach focuses, for simplicity, on a single microgel carrying a fixed charge that is independent of system properties, it does not directly describe release of quasi-bound counterions in response to changes of concentration. A multi-center model of microgel suspensions that includes microgel-microgel interactions may be a basis for incorporating a concentration-dependent fixed charge, using concepts of charge renormalization with a thermal definition of effective fixed charge.<sup>76</sup> While such an approach is

beyond the scope of the present study, it may be worth exploring in future. Nevertheless, our theoretical predictions and simulations do indicate stronger aggregation of counterions near the charged microgel surface with increasing concentration (Fig. 3), which might be related to quasi-binding of counterions in a more molecular-scale model. Figure 3 further shows that the counterion number density at the cell edge increases with concentration, suggesting increasing overlap of the counterion clouds surrounding neighboring microgels, consistent with the conceptual picture presented in Refs. 56–58.

We note that our results for counterion number density profiles are qualitatively similar to those reported in a related study of surface-charged ionic microgels, <sup>58</sup> in which the PB equation was numerically solved in the cell model. However, our conclusions regarding equilibrium swelling differ significantly from those in Ref. 58, where the electrostatic component of the single-microgel osmotic pressure was determined from the microion number density at the center of the cell, implying [from Eq. (22)]

$$\beta \pi_e = n_+(0) + n_-(0) = 2n_0 \cosh \left[ \psi(0) \right]. \tag{29}$$

The latter approximation, although valid in planar geometry (e.g., for a flat film), neglects nonuniformity of the elements of the pressure tensor in curvilinear geometry. In spherical geometry, for example, the normal (radial) element of the pressure tensor,  $P_m(r)$ , varies with radial distance. As described in detail elsewhere, this property follows from the requirement that the divergence of the pressure tensor vanish in mechanical equilibrium. In particular, for a surface-charged microgel in the spherical cell model, the normal element of the electrostatic pressure tensor,  $P_e(r)$ , is higher at the microgel surface than at the center (see Fig. 14 of Ref. 22). As a consequence, Eq. (29) actually represents the normal element of the electrostatic pressure at the microgel center,  $P_e(0)$ , rather than the electrostatic component of the single-microgel osmotic pressure  $\pi_e$ . Furthermore,  $P_e(0)$  is generally significantly lower than  $\pi_e$ .

In equilibrium, the normal element of the gel contribution to the pressure tensor,  $P_g(r)$ , must counteract the electrostatic contribution,  $P_e(r)$ , to mechanically stabilize the fixed charge against the electric field  $(-\psi')$ . For a fixed charge density  $n_f(r)$ , a simple mechanical argument yields the gel contribution as<sup>22</sup>

$$P_g(r) = -\int_r^R du n_f(u) \psi'(u). \tag{30}$$

In general,  $P_g(r) = 0$  outside the microgel, where  $n_f = 0$ , and is spatially varying inside. For our particular model of a surface-charged microgel, with  $n_f(r)$  given explicitly by a Dirac delta-function [Eq. (1)], Eq. (30) yields<sup>22</sup>

$$P_g(r) = -\frac{Z}{8\pi a^2} \lim_{\delta \to 0} \left[ \psi'(a+\delta) + \psi'(a-\delta) \right] = -\pi_e.$$
 (31)

Thus, for a surface-charged microgel,  $P_g(r)$  jumps discontinuously at the surface from zero to a value equal to the negative of the electrostatic component of the single-microgel osmotic pressure, and remains constant at that value inside the microgel. In contrast,  $P_e(r)$  and  $P_m(r)$  vary with radial distance due to the spherical geometry.

To illustrate the difference between our approach and that of Ref. 58, Fig. 6 plots the normal element of the pressure tensor in

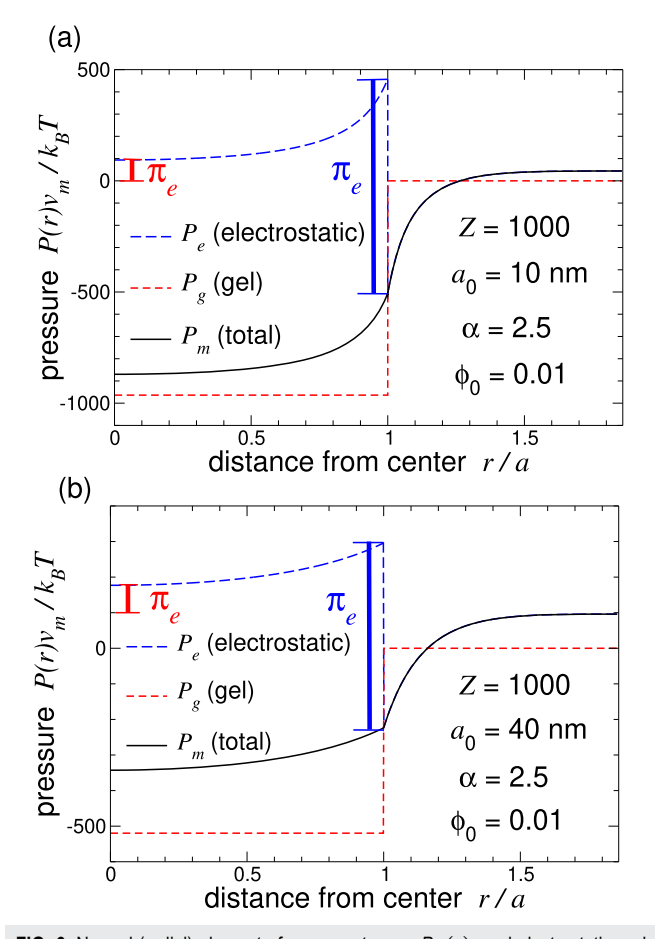


**FIG. 6.** Normal (radial) element of pressure tensor,  $P_m(r)$ , and electrostatic and gel contributions,  $P_e(r)$  and  $P_g(r)$ , respectively, where  $P_m(r) = P_e(r) + P_g(r)$ , for a surface-charged microgel in the spherical cell model with dry volume fraction  $\phi_0 = 0.01$ , swelling ratio  $\alpha = 2.5$ , and dry and swollen radii (a)  $a_0 = 10$  nm, a = 25 nm and (b)  $a_0 = 40$  nm, a = 100 nm. Thick red and blue vertical lines have lengths representing the value of  $\pi_e$  predicted, respectively, by Eq. (29)  $^{58}$  and our Eq. (19) or, equivalently, (27).

the spherical cell model for the case  $\phi_0 = 0.01$ ,  $\alpha = 2.5$ , separately showing the electrostatic and gel contributions, computed using the methods from Ref. 22. Panel (a) is for the case of microgels with dry and swollen radii  $a_0 = 10$  nm and a = 25 nm, respectively; panel (b) is for  $a_0 = 40$  nm and a = 100 nm, which is closer to the experimental system studied in Ref. 58. The thick blue vertical line has a length equaling our result for  $\pi_e$ , while the thick red vertical line length represents the value predicted by Eq. (29). Evidently, the two approaches make substantially different predictions. In fact, when we use Eq. (29), instead of our Eq. (19) [equivalently, Eq. (27)] to compute equilibrium swelling ratios for the case of  $a_0 = 10$  nm, we find that  $\alpha$  varies only slightly with  $\phi_0$ , actually increasing from 2.355 at  $\phi_0 = 0.01$  to 2.358 at  $\phi_0 = 0.05$ . In contrast, our approach, which is consistent with nonuniformity of the pressure tensor,<sup>22</sup> predicts  $\alpha$  decreases from 3.03 at  $\phi = 0.01$  to 2.37 at  $\phi_0 = 0.05$  for this system (Fig. 5).

Of particular interest here is a direct comparison between equilibrium swelling of surface- and volume-charged microgels. As illustrated in Fig. 5, with increasing concentration, surface-charged microgels deswell significantly more rapidly than volume-charged microgels that have otherwise the same particle properties. This trend can be attributed in part to the lower self-energy of surface-charged microgels,  $\beta U_m = Z^2 \lambda_B/(2a)$ , compared with  $\beta U_m = 3Z^2 \lambda_B/(5a)$  for volume-charged microgels. However, the counterion density distribution also clearly plays a role in lowering the electrostatic osmotic pressure, which suppresses swelling.

Intermediate between the extremes of surface- and volume-charged microgels are microgels with the same fixed charge uniformly distributed over the volume of a peripheral spherical shell. In previous work on ionic microcapsules (hollow microgels),  $^{62,63}$  we derived an expression for the self-energy of a charged spherical shell with inner and outer radii  $R_i$  and  $R_o$ , respectively:

$$\beta U_m(R_o, \gamma) = \frac{3Z^2 \lambda_B}{10R_o} \frac{2 - 5\gamma^3 + 3\gamma^5}{(1 - \gamma^3)^2},$$
 (32)

where  $y \equiv R_i/R_0 \le 1$ . With increasing shell thickness (i.e., decreasing y),  $U_m$  from Eq. (32) *increases*, exceeding  $U_m$  for a surface-charged microgel [Eq. (4)], and approaching the result for a volume-charged microgel as  $y \to 0$ . Thus, spreading the fixed charged over the volume of a spherical shell would increase electrostatic self-energy and thereby tend to promote swelling.

Finally, we explore the response of ionic microgels to changes in salt concentration. For two different system salt concentrations,  $c_s = 10$  and 20 mM, we numerically solved the PB equation [Eq. (23)] for both counterion and coion density profiles  $n_{\pm}(r)$ , from which we computed the electrostatic component of the single-microgel osmotic pressure from Eq. (19) and equilibrium swelling ratios from Eq. (13). Figure 7 shows the resulting variation of equilibrium swelling ratio with microgel concentration for the same system

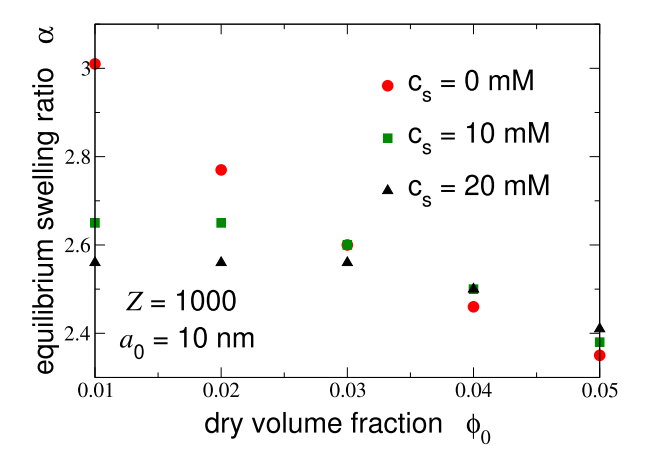


**FIG. 7.** Equilibrium swelling ratio  $\alpha$  vs dry volume fraction  $\phi_0$  for surface-charged microgels of valence Z=1000 and dry radius  $a_0=10$  nm in aqueous suspensions with system salt concentrations  $c_{\rm s}=0$  (red circles), 10 mM (green squares), and 20 mM (black triangles). Over this range of  $\phi_0$ , the swollen volume fraction,  $\phi=\alpha^3\phi_0$ , varies (nonlinearly) from about 0.28–0.67 for surface-charged microgels and the fixed charge concentration  $c_f$  varies from about 4–20 mM.

parameters as in Fig. 3. Over this range of dry volume fraction,  $0.01 < \phi_0 < 0.05$ , the average concentration of fixed charge,

$$c_f = \frac{3Z}{4\pi} \frac{\phi_0}{(a_0 \lceil \text{nm} \rceil)^3} \frac{1 \text{mM}}{6.022 \times 10^{-4} \text{ nm}^{-3}},$$
 (33)

varies from about 4–20 mM. Since  $c_f$ , and thus also the counterion concentration, is comparable in magnitude to the salt concentration, some significant response of swelling to variation of  $c_s$  may be expected. At higher salt concentrations, the nonlinear PB equation becomes so numerically stiff that our differential equation solver unfortunately fails. However, even for  $c_s \le 20$  mM, we already observe a significant influence of added salt on microgel swelling.

In relatively dilute suspensions ( $\phi_0$  < 0.03), microgels typically respond to increasing salt concentration by deswelling. This response is conventionally attributed to enhanced screening of the microgel fixed charge upon increasing the overall concentration of microions and the attendant suppression of electrostatic-driven swelling. Another interpretation is suggested, however, by close inspection of the expression for the electrostatic component of the single-microgel osmotic pressure [Eq. (19)]. Adding salt ion pairs to the suspension leads on average to microgels preferentially absorbing counterions over coions (i.e.,  $\langle N_+ \rangle$  rises more than  $\langle N_- \rangle$ ). Dilute suspensions provide ample free volume outside of the microgels in which coions can minimize their energetically costly interactions with microgel surfaces. With the electrostatic component of the osmotic pressure being thus weakened, the gel component favors a lower swelling ratio.

In more concentrated suspensions ( $\phi_0 > 0.03$ ), we observe an interesting reversal in the swelling response, with crowded microgels swelling slightly upon adding salt. This unusual response implies that highly crowded microgels, which already harbor a significant concentration of counterions, tend to engulf more of any added coions than added counterions. This trend is perhaps not surprising, considering that in crowded suspensions, where free volume outside of the microgels is limited, exterior coions are constrained to be relatively close to the like-charged microgel surfaces, where they must pay a higher energetic cost of interaction. In contrast, by moving inside a microgel, a coion can avoid the charged surface, while also reducing energy by gaining proximity to oppositely-charged counterions. Swelling of microgels further favors coions remaining inside the microgels. This result illustrates the complex nature of the electrostatic component of the single-microgel osmotic pressure, which involves a delicate balance between the mean numbers of counterions and coions inside the microgels.

Whether the swelling trend observed with increasing salt concentration would continue to higher microgel concentrations is an interesting question. Unfortunately, our cell-model approach is unable to provide a clear answer, since  $\phi_0=0.05$  already approaches a swollen volume fraction at which elastic interactions between neighboring microgels would start to become important. This question could be addressed, however, within a multi-center model that includes microgel-microgel interactions.  $^{42}$  Finally, we note that, despite the qualitatively different swelling behavior of ionic microgels as compared with that of bulk ionic gels, our approach has in common with theories of bulk gels  $^{17-20}$  that it associates swelling with osmotic pressure – albeit that of a single microgel – which is

intimately related to microion distributions inside and outside of the gel.

## VI. CONCLUSIONS

Within the primitive and cell models of permeable, compressible, ionic microgels, we investigated the dependence of single-particle osmotic pressure and equilibrium swelling on the distribution of fixed charge over the cross-linked polymer network making up the particles. Applying an exact theorem for the electrostatic component of the single-particle osmotic pressure – implemented within Poisson–Boltzmann theory and validated via molecular dynamics simulations – and modeling the gel component using Flory–Rehner theory of polymer networks, we computed equilibrium swelling ratios of microgels (with monovalent counterions) whose fixed charge is confined to and uniformly distributed over their surfaces.

Our study demonstrates that the osmotic pressure and swelling properties of ionic microgels are strongly dependent on the fixed charge distribution through its influence on the microgel electrostatic self-energy and the microion density profiles. Our results further indicate that surface-charged microgels deswell significantly more strongly with increasing concentration (i.e., crowding) than microgels that carry a fixed charge uniformly distributed over their volume. Results for these two idealized models may serve to bracket the swelling behavior to be expected of ionic microgels with intermediate fixed charge distributions. Finally, we found that, with increasing salt concentration, swelling of surface-charged microgels in dilute suspensions is suppressed, due to enhanced screening of bare Coulomb electrostatic interactions, but that the effect is weaker, or can even invert, in more concentrated suspensions.

Although our study is restricted to suspensions of relatively idealized model microgels with uniform cross-link densities and fixed charges evenly distributed over their surfaces or volumes, our results vividly reveal the importance of fixed charge distribution for single-particle osmotic pressure and equilibrium swelling. Further increasing the salt concentration or varying counterion and microgel valences may significantly modify electrostatically-driven swelling. Steric interactions associated with nonzero microion size also may be important. While such effects are beyond the scope of the present mean-field modeling approach, they would be well worth exploring in future.

Our conclusions regarding the influence of fixed charge distribution on swelling are qualitatively consistent with experimental measurements of ionic microgels and can be further tested in experiments (e.g., light or neutron scattering) on microgels produced via synthesis protocols that yield varying distributions of fixed charge. Thus, our results may provide insights into swelling behavior and guide practical approaches to controlling swelling of microgels for practical applications. In future work, we will explore structural properties of bulk suspensions of surface-charged ionic microgels and of mixtures thereof with size and charge asymmetry.

# **ACKNOWLEDGMENTS**

We thank Mariano Brito, Gerhard Nägele, Jan Dhont, and Andrea Scotti for helpful discussions. M.O.A. acknowledges Shaqra University for financial support. A.R.D. acknowledges support of the National Science Foundation (Grant No. DMR-1928073).

#### **AUTHOR DECLARATIONS**

## **Conflict of Interest**

The authors have no conflicts to disclose.

## **Author Contributions**

Mohammed O. Alziyadi: Data curation (lead); Formal analysis (lead); Software (equal); Writing – original draft (lead); Writing – review & editing (supporting). Alan R. Denton: Conceptualization (lead); Data curation (equal); Formal analysis (equal); Funding acquisition (lead); Methodology (equal); Project administration (lead); Resources (lead); Software (equal); Supervision (lead); Validation (equal); Writing – original draft (supporting); Writing – review & editing (lead).

# **DATA AVAILABILITY**

The data that support the findings of this study are available from the corresponding author upon reasonable request.

## **REFERENCES**

- <sup>1</sup> Microgel Suspensions: Fundamentals and Applications, edited by A. Fernández-Nieves, H. Wyss, J. Mattsson, and D. A. Weitz (Wiley-VCH Verlag GmbH & Co. KGaA, Weinheim, 2011).
- <sup>2</sup> Hydrogel Micro and Nanoparticles, edited by L. A. Lyon and M. J. Serpe (Wiley-VCH Verlag GmbH & Co. KGaA, Weinheim, 2012).
- <sup>3</sup>M. Karg, A. Pich, T. Hellweg, T. Hoare, L. A. Lyon, J. J. Crassous, D. Suzuki, R. A. Gumerov, S. Schneider, I. I. Potemkin, and W. Richtering, Langmuir 35, 6231 (2019).
- <sup>4</sup>A. Scotti, M. F. Schulte, C. G. Lopez, J. J. Crassous, S. Bochenek, and W. Richtering, Chem. Rev. 122, 11675 (2022).
- <sup>5</sup>R. Pelton and T. Hoare, in *Microgel Suspensions: Fundamentals and Applications*, edited by A. Fernández-Nieves, H. Wyss, J. Mattsson, and D. A. Weitz (Wiley-VCH Verlag GmbH & Co. KGaA, Weinheim, 2011), pp. 3–32.
- <sup>6</sup>B. Sierra-Martin, J. J. Lietor-Santos, A. Fernandez-Barbero, T. T. Nguyen, and A. Fernandez-Nieves, "Swelling thermodynamics of microgel particles," in *Microgel Suspensions: Fundamentals and Applications* (Wiley-VCH Verlag GmbH & Co. KGaA, Weinheim, 2011), pp. 71–116.
- <sup>7</sup>P. J. Flory, *Principles of Polymer Chemistry* (Cornell University Press, Ithaca, 1052)
- <sup>8</sup>H. M. Wyss, J. Mattsson, T. Franke, A. Fernández-Nieves, and D. A. Weitz, in *Microgel Suspensions: Fundamentals and Applications*, edited by A. Fernández-Nieves, H. Wyss, J. Mattsson, and D. A. Weitz (Wiley-VCH Verlag GmbH & Co. KGaA, Weinheim, 2011), pp. 311–326.
- <sup>9</sup> A. Fernández-Nieves, A. Fernández-Barbero, B. Vincent, and F. J. de las Nieves, J. Chem. Phys. **119**, 10383 (2003).
- <sup>10</sup>C. N. Likos, in *Microgel Suspensions: Fundamentals and Applications*, edited by A. Fernández-Nieves, H. Wyss, J. Mattsson, and D. A. Weitz (Wiley-VCH Verlag GmbH & Co. KGaA, Weinheim, 2011), pp. 165–193.
- <sup>11</sup>G. Romeo, L. Imperiali, J.-W. Kim, A. Fernández-Nieves, and D. A. Weitz, J. Chem. Phys. **136**, 124905 (2012).
- <sup>12</sup>E. Pashkovski, in *Microgel Suspensions: Fundamentals and Applications*, edited by A. Fernández-Nieves, H. Wyss, J. Mattsson, and D. A. Weitz (Wiley-VCH Verlag GmbH & Co. KGaA, Weinheim, 2011), pp. 423–450.

- <sup>13</sup>M. Malmsten, in Microgel Suspensions: Fundamentals and Applications, edited by A. Fernández-Nieves, H. Wyss, J. Mattsson, and D. A. Weitz (Wiley-VCH Verlag GmbH & Co. KGaA, Weinheim, 2011), pp. 375-405.
- <sup>14</sup>Y. Ben, I. Robb, P. Tonmukayakul, and Q. Wang, in Microgel Suspensions: Fundamentals and Applications, edited by A. Fernández-Nieves, H. Wyss, J. Mattsson, and D. A. Weitz (Wiley-VCH Verlag GmbH & Co. KGaA, Weinheim, 2011), pp. 407–422. <sup>15</sup> J. Tavakoli and Y. Tang, Polymers **9**, 364 (2017).
- <sup>16</sup>M. Hamidi, A. Azadi, and P. Rafiei, Adv. Drug Delivery Rev. **60**, 1638 (2008).
- <sup>17</sup>I. Ohmine and T. Tanaka, J. Chem. Phys. 77, 5725 (1982).
- <sup>18</sup>J. Ricka and T. Tanaka, Macromolecules 17, 2916 (1984).
- <sup>19</sup>R. A. Siegel and B. A. Firestone, Macromolecules 21, 3254 (1988).
- <sup>20</sup>J.-L. Barrat, J.-F. Joanny, and P. Pincus, J. Phys. II **2**, 1531 (1992).
- <sup>21</sup> A. R. Denton and Q. Tang, J. Chem. Phys. **145**, 164901 (2016).
- <sup>22</sup> A. R. Denton and M. O. Alziyadi, J. Chem. Phys. **151**, 074903 (2019).
- <sup>23</sup> A. Fernández-Nieves, A. Fernández-Barbero, B. Vincent, and F. J. de las Nieves, Macromolecules 33, 2114 (2000).
- <sup>24</sup>P. S. Mohanty and W. Richtering, J. Phys. Chem. B 112, 14692 (2008).
- <sup>25</sup>P. Holmqvist, P. S. Mohanty, G. Nägele, P. Schurtenberger, and M. Heinen, Phys. Rev. Lett. 109, 048302 (2012); Erratum 117, 179901 (2016).
- <sup>26</sup>M. Braibanti, C. Haro-Pérez, M. Quesada-Pérez, L. F. Rojas-Ochoa, and V. Trappe, Phys. Rev. E 94, 032601 (2016).
- <sup>27</sup>M. Stieger, W. Richtering, J. S. Pedersen, and P. Lindner, J. Chem. Phys. 120,
- <sup>28</sup>J. J. Liétor-Santos, U. Gasser, R. Vavrin, Z. B. Hu, and A. Fernández-Nieves, J. Chem. Phys. 133, 034901 (2010).
- <sup>29</sup>S. Nöjd, P. Holmqvist, N. Boon, M. Obiols-Rabasa, P. S. Mohanty, R. Schweins, and P. Schurtenberger, Soft Matter 14, 4150 (2018).
- 30 B. Zhou, U. Gasser, and A. Fernandez-Nieves, Nat. Commun. 14, 3827 (2023).
- 31 M. Pelaez-Fernandez, A. Souslov, L. A. Lyon, P. M. Goldbart, and A. Fernández-Nieves, Phys. Rev. Lett. 114, 098303 (2015).
- 32 A. Scotti, M. Pelaez-Fernandez, U. Gasser, and A. Fernandez-Nieves, Phys. Rev. E 103, 012609 (2021).
- <sup>33</sup>P. S. Mohanty, S. Nöjd, M. J. Bergman, G. Nägele, S. Arrese-Igor, A. Alegria, R. Roa, P. Schurtenberger, and J. K. G. Dhont, Soft Matter 12, 9705 (2016).
- <sup>34</sup>R. Borrega, M. Cloitre, I. Betremieux, B. Ernst, and L. Leibler, Europhys. Lett. 47, 729 (1999).
- 35 M. Cloitre, R. Borrega, F. Monti, and L. Leibler, C. R. Phys. 4, 221 (2003).
- <sup>36</sup>Y. Levin, A. Diehl, A. Fernández-Nieves, and A. Fernández-Barbero, Phys. Rev. E 65, 036143 (2002).
- <sup>37</sup>J. Riest, P. Mohanty, P. Schurtenberger, and C. N. Likos, Z. Phys. Chem. 226, 711 (2012).
- <sup>38</sup>T. Colla, C. N. Likos, and Y. Levin, J. Chem. Phys. **141**, 234902 (2014).
- <sup>39</sup> A. Moncho-Jordá, J. Chem. Phys. **139**, 064906 (2013).
- <sup>40</sup> A. R. Denton, Phys. Rev. E **67**, 011804 (2003); Erratum **68**, 049904 (2003).
- <sup>41</sup>D. Gottwald, C. N. Likos, G. Kahl, and H. Löwen, J. Chem. Phys. 122, 074903
- <sup>42</sup>T. J. Weyer and A. R. Denton, Soft Matter **14**, 4530 (2018).
- <sup>43</sup>L. A. Aguirre-Manzo, M. Ledesma-Motolinía, L. F. Rojas-Ochoa, V. Trappe, J. Callejas-Fernández, C. Haro-Pérez, and P. González-Mozuelos, Phys. Rev. E 100, 032602 (2019).

- <sup>44</sup>M. E. Brito, A. R. Denton, and G. Nägele, J. Chem. Phys. **151**, 224901 (2019).
- <sup>45</sup>M. M. Hedrick, J. K. Chung, and A. R. Denton, J. Chem. Phys. **142**, 034904 (2015)
- 46 H. Kobayashi and R. G. Winkler, Polymers 6, 1602 (2014).
- <sup>47</sup> A. Ghavami and R. G. Winkler, ACS Macro Lett. **6**, 721 (2017).
- <sup>48</sup>P. S. Mohanty, D. Paloli, J. J. Crassous, E. Zaccarelli, and P. Schurtenberger, J. Chem. Phys. 140, 094901 (2014).
- <sup>49</sup>N. Gnan, L. Rovigatti, M. Bergman, and E. Zaccarelli, Macromolecules **50**, 8777
- <sup>50</sup>S. Schneider and P. Linse, Eur. Phys. J. E **8**, 457 (2002).
- <sup>51</sup> M. Quesada-Pérez and A. Martín-Molina, Soft Matter **9**, 7086 (2013).
- 52C. Hofzumahaus, P. Hebbeker, and S. Schneider, Soft Matter 14, 4087
- <sup>53</sup> M. Urich and A. R. Denton, Soft Matter **12**, 9086 (2016).
- <sup>54</sup>P. S. Mohanty, A. Yethiraj, and P. Schurtenberger, Soft Matter **8**, 10819
- <sup>55</sup>N. Boon and P. Schurtenberger, Phys. Chem. Chem. Phys. 19, 23740 (2017).
- <sup>56</sup> A. Scotti, U. Gasser, E. S. Herman, M. Pelaez-Fernandez, J. Han, A. Menzel, L. A. Lyon, and A. Fernández-Nieves, Proc. Natl. Acad. Sci. U. S. A. 113, 5576
- <sup>57</sup>A. Scotti, U. Gasser, E. S. Herman, J. Han, A. Menzel, L. A. Lyon, and A. Fernández-Nieves, Phys. Rev. E 96, 032609 (2017).
- <sup>58</sup>U. Gasser, A. Scotti, and A. Fernández-Nieves, Phys. Rev. E **99**, 042602 (2019).
- <sup>59</sup> J. Zhou, J. Wei, T. Ngai, L. Wang, D. Zhu, and J. Shen, Macromolecules **45**, 6158
- <sup>60</sup>M. Deserno and C. Holm, in Electrostatic Effects in Soft Matter and Biophysics, NATO Advanced Studies Institute Series II: Mathematics Physics and Chemistry Vol. 46, edited by C. Holm, P. Kékicheff, and R. Podgornik (Kluwer, Dordrecht, 2001), pp. 27-50.
- <sup>61</sup> A. R. Denton, in *Electrostatics of Soft and Disordered Matter*, edited by D. S. Dean, J. Dobnikar, A. Naji, and R. Podgornik (Pan Stanford, Singapore, 2014), pp. 201-215.
- 62 S. K. Wypysek, A. Scotti, M. O. Alziyadi, I. I. Potemkin, A. R. Denton, and W. Richtering, Macromol. Rapid Commun. 41, 1900422 (2019).
- 63 M. O. Alziyadi and A. R. Denton, J. Chem. Phys. 155, 214904 (2021).
- <sup>64</sup>N. W. Ashcroft and N. D. Mermin, *Solid State Physics* (Holt-Saunders, Fort Worth, 1976).
- 65 C. Kittel, Introduction to Solid State Physics (Wiley, Hoboken, 2004).
- <sup>66</sup>R. A. Marcus, J. Chem. Phys. 23, 1057 (1955).
- <sup>67</sup>G. C. Claudio, K. Kremer, and C. Holm, J. Chem. Phys. **131**, 094903 (2009).
- <sup>68</sup> H. Wennerström, B. Jönsson, and P. Linse, J. Chem. Phys. 76, 4665 (1982).
- <sup>69</sup>P. J. Flory and J. Rehner, J. Chem. Phys. **11**, 512 (1943).
- <sup>70</sup> P. J. Flory and J. Rehner, J. Chem. Phys. **11**, 521 (1943).
- <sup>71</sup> E. Trizac and J.-P. Hansen, Phys. Rev. E **56**, 3137 (1997).
- $^{\bf 72}{\rm A.}$  Widom, J. Swain, J. Silverberg, S. Sivasubramanian, and Y. N. Srivastava, Phys. Rev. E 80, 016301 (2009).
- 73 H. Löwen, P. A. Madden, and J.-P. Hansen, Phys. Rev. Lett. 68, 1081 (1992).
- <sup>74</sup>See http://lammps.sandia.gov for information about the large-scale atomic/ molecular massively parallel simulator (LAMMPS) package.
- <sup>75</sup>S. Plimpton, J. Comput. Phys. **117**, 1 (1995).
- <sup>76</sup> A. R. Denton, J. Phys.: Condens. Matter **22**, 364108 (2010).